CHAPTER 37

THE PS AND TRANSFER LINE TO SPS

37.1 INJECTION: TRAJECTORIES AND OPTICS

Partially stripped Pb^{54+} ion beam will be injected into the PS ring at 72.2 MeV/u. The selected LEIR extraction energy is a compromise between the incoherent tune shift limit at PS injection ($\Delta Q_{inc} < 0.25$), the bunch spacing needed for the ejection kicker rise time, the cycle length in LEIR and the minimum frequency attainable with the PS RF system [1, 2]. Tab. 37.1 summarizes the main parameters of lead ion beams at transfer between LEIR and PS and at PS extraction for the sake of completeness.

Table 37.1: Summary of lead ion beam characteristics at PS input and output.

Parameter at PS	Injection	Ejection
Kinetic energy	72.16 MeV/u	5.88 GeV/u
Proton kinetic energy for equal Bρ	779.60 MeV	25.06 GeV
γ	1.077	7.312
β	0.372	0.991
Beam rigidity (Bρ)	4.80 Tm	86.67 Tm
Magnetic field in PS dipoles	0.0685 T	1.237 T
Number of injected bunches	2 every 3.6 s	8 "bunchlets"
Number of Pb^{54+} ions per batch	9.0×10^8	4.8×10^8
Normalised transverse emittance (1σ)	0.7 μm	1.0 μm

37.1.1 Layout of the Former Antiproton PS Extraction towards LEAR

The former PS antiproton ejection to LEAR took place in the long PS straight-section 26 as depicted in Fig. 37.1.

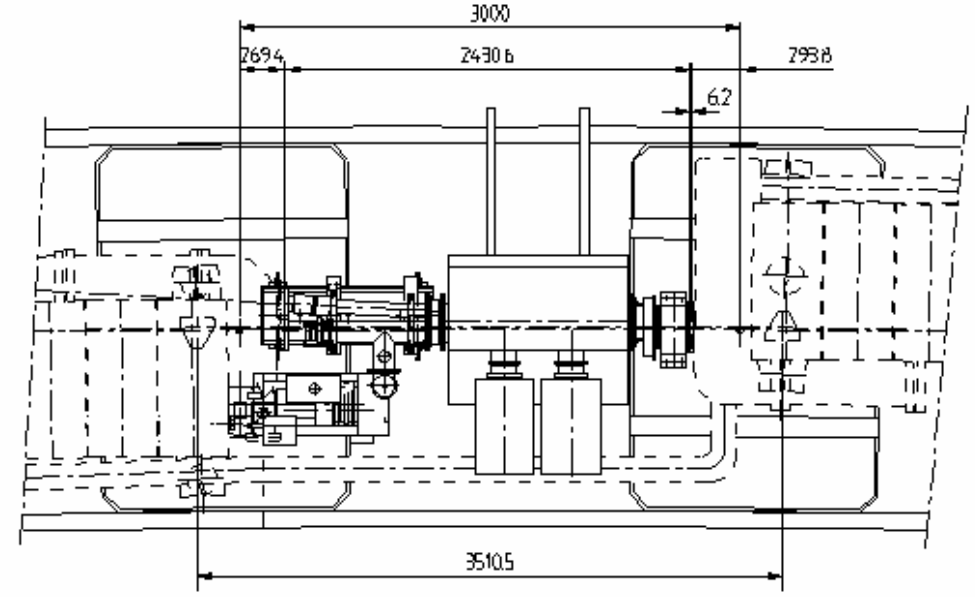

Figure 37.1: Layout of the PS straight-section 26 with the antiproton extraction septum.

Antiprotons were fast extracted from the PS at 2.0 Tm beam rigidity using kicker and septum magnets located in straight-sections 28 and 26. The septum strength used in operation to extract the beam ($\int Bdl = 0.105$ Tm gave a deflection angle of 51.5 mrad) did not exceed the maximum attainable value of 0.117 Tm. No local closed orbit distortion was needed since the kicker strength necessary to eject directly

from the central orbit (∫Bdl=192.6 Gm yielding a kick of 9.5 mrad) was below the maximum kicker value of 232.4 Gm. Beam position and angle at the septum were 80.6 mm and 6.7 mrad respectively. The septum was positioned at 53 mm from the central orbit; its thickness varies between 1.5 mm and 18 mm. Fig. 37.2 shows the Y shape vacuum chamber adjacent to the ejection septum tank used to take the antiproton beam out of the PS ring.

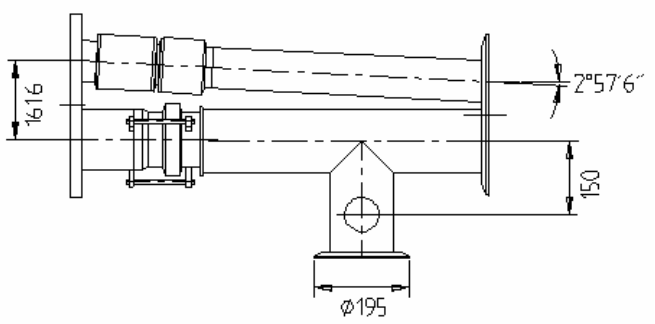

Figure 37.2: Y shape vacuum chamber adjacent to the extraction septum 26. The angle between the two pipes is 2°57′6″ or 51.5 mrad, the nominal extracted antiproton deflection angle.

37.1.2 Lead Ion Injection Scenario into the PS

The lead ion beams from LEIR will follow the geometry of the former antiproton transfer line in the reverse direction. The higher ion beam rigidity (4.8 Tm) would require septum magnet strength of 0.247 Tm to handle the 51.5 mrad beam deflection, which is beyond the maximum strength of the present septum (0.117 Tm). A new septum for ion injection with a maximum strength of 0.264 Tm has then been proposed. From the geometry of the Y shaped injection pipe the beam position at the septum 26 centre is evaluated to be 84.3 mm. Pushing the beam onto the reference orbit from the 84.3 mm beam position at the septum would need a kicker strength of 469.8 Gm (9.8 mrad kick), a little bit too high even if the present kicker strength is upgraded (Bdl_{max}=464.8 Gm).

A local closed orbit bump is proposed to push the beam towards the septum. With the upgraded kicker a local closed orbit bump is not strictly needed but still recommended in order to keep some margin. The bump must not exceed the distance of the septum from the central orbit minus the half-width of the injected beam and possible orbit distortions. The horizontal beam size (at 6σ) near the septum is of the order of 30 mm. Assuming the same 53 mm septum position used for the former antiproton extraction, and taking a 13 mm safety margin for orbit distortions and kicker tuning, the bump at the septum is found to be 25 mm. A three-magnet bump creates the needed orbit displacement without residual orbit deformation outside the injection region. This bump can be reduced to an almost half-wavelength two-magnet bump if a small residual orbit distortion outside the bump is permitted.

Three-magnet bump

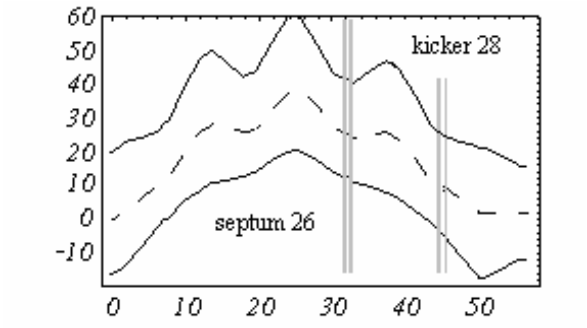

Figure 37.3: Three-dipole bump with 6σ-beam envelope [mm] in PS straight-sections 21, 25, 29. The dipoles are at 0.2 m, 25.1 m, 50.0 m from the centre of straight-section 21.

Fig. 37.3 shows a three-magnet bump with 25 mm amplitude at the septum. The phase advance between the dipoles 29 and 21 is very close to π. The three kicks producing the bump are below 2 mrad, the maximum strength of the deflecting dipoles being 86 Gm. The kicker 28 is inside the bump extension so that the orbit is displaced by 10 mm in the kicker tank.

Fig. 37.4 shows the injected beam envelope (at 6σ) from a matching point in the LEIR to PS transfer line (located 6.5 m upstream from the septum centre) to the kicker 28, together with that of the circulating beam over the range of the bump. The 38 mm maximum displacement of the beam is reached in straight-section 25, at about 25 m from the beginning of the bump while the maximum beam size coordinate on the outside is 58 mm within straight-section 25. The kicker 28 strength has to be enhanced from 232.4 to 330.4 Gm.

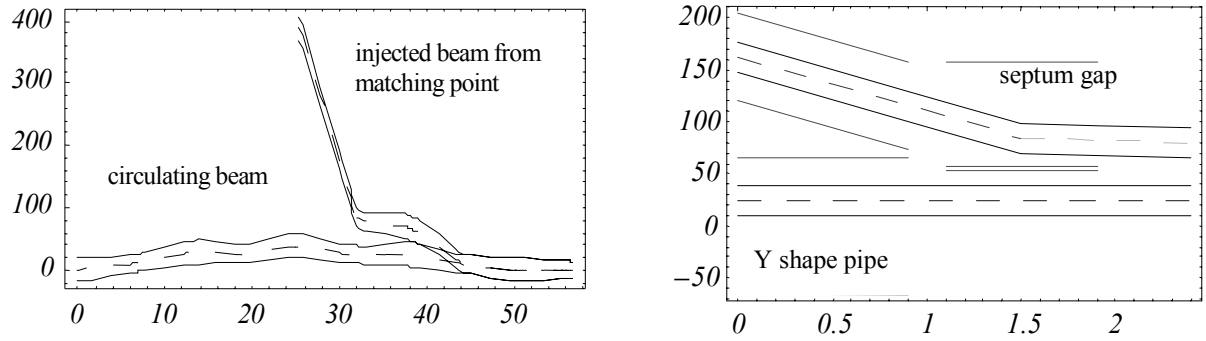

Figure 37.4: Left: horizontal injected and circulating 6σ-beam envelopes over the full bump range [mm]. Right: horizontal 6σ-beam envelopes in PS straight-section 26 [mm].

Two-magnet bump

The best configuration for the position of the dipoles, given the smaller residual orbit distortion outside the bump region, is a symmetric two-magnet bump with dipoles in straight-sections 22 and 30. The phase difference between the dipoles is very close to π. The required kick is 2.1 mrad per dipole yielding a residual orbit distortion of about 2 mm.

37.1.3 Matching Conditions between LEIR Output and PS Input

The PS magnet unit 25 adjacent to septum 26 is made of a closed half-unit followed by an open half-unit. The incoming beam trajectories pass far from the central orbit of the closed half-unit (at about 430 mm on average), where the gradient has a reverse polarity, and about 250 mm away from the open half-unit. The incoming beam will thus experience the stray field of the magnet.

PS magnet field map values have been obtained from magnetic measurements at 3.5 GeV/c [3]. The gradient and thus the deflecting field away from the central orbit may be derived from these data by interpolation and extrapolation using approximation formulas for the fringe field [4]. The mean gradient and deflection angle seen by the input beam in the closed and open half-units are -0.008 m^{-2}, 2.2 mrad and -0.020 m^{-2}, 5.1 mrad, respectively. These values have to be compared to the nominal ±0.059 m^{-2} and 31.4 mrad gradient and angle on the central orbit. The resulting transfer matrices in the LEIR to PS transfer line, from the magnet unit 25 stray field entry (matching point M) to septum 26 centre have been derived accordingly. Optical parameters at point M are obtained propagating back the required optical parameters at injection point (septum centre) through the transfer line from the septum up to point M (Tab. 37.2).

Table 37.2: Parameters at PS septum and LEIR to PS transfer line point M (located 6.5 m away).

Optical parameters	β_x [m]	α_x	β_y [m]	α_y	D_x [m]	D'_x	D_y [m]	D'_y
PS septum 26 centre	12.48	0	19.71	0	2.21	-0.02	0	0
LEIR-PS matching point	21.50	1.62	15.21	-0.71	2.78	-0.17	0	0

37.1.4 Hardware for PS Ion Injection

The three-magnet orbit bump as well as the simpler two-magnet bump (using one power supply only) are presented in Tab. 37.3. The two-magnet bump will be implemented first with the possibility to install a 3-magnet bump later if needed. A new injection septum has to be built and the present kicker 28 must be upgraded to handle ion beams with 4.8 Tm beam rigidity (Tab. 37.4).

Table 37.3: PS injection dipole bump characteristics.

Dipole location in PS straight-sections	Dipole deflection angle	Maximum bump amplitude	Remarks
3-dipole bump in PS sections 21-25-29	1.8, -0.1, 1.7 mrad (max 86 Gm)	38 mm in straight section 25	no residual orbit, needs 3 power supplies
2-dipole bump in PS sections 22-30	2.1, 2.1 mrad (max 100 Gm)	32 mm in straight sections 25-27	about 2 mm residual closed orbit, needs 1 power supply

Table 37.4: PS injection septum and kicker characteristics.

Magnet type	Integrated magnetic field for 4.8 Tm lead ion injection	Foreseen maximum integrated magnetic field
Septum 26	0.247 Tm (51.5 mrad)	0.264 Tm
Kicker 28 with a 25 mm bump	330.4 Gm (6.9 mrad)	464.8 Gm (2×232.4)

37.2 NEW PULSED INJECTION SEPTUM

The LEIR extraction energy requires a new magnetic septum in the PS for the injection of the ions. The main parameters of the septum for a particle beam with a magnetic rigidity of $B\rho = 4.8$ Tm are indicated in Tab. 37.5. The vacuum tank, the mechanical support structure, the vacuum equipment and the magnet displacement systems, together with their spare, are recovered from the "PE.SMH58" device (previously used for electron extraction in the PS ring) to reduce the cost. The spare has never been installed in the PS, and thus is not radioactive. These existing vacuum tanks are modified to contain the magnet and to fit into straight section 26. New magnets have been constructed and their design is based on the septa previously developed for the PSB to PS transfer line, keeping their cross section, but modifying the length to suit the present application. However, the modification of the existing vacuum vessel that has been installed in the PS ring from 1994 to early 2003 was done very carefully, because it is slightly radioactive. Modifications are required to ensure compatibility between the tank and the existing PS vacuum chamber.

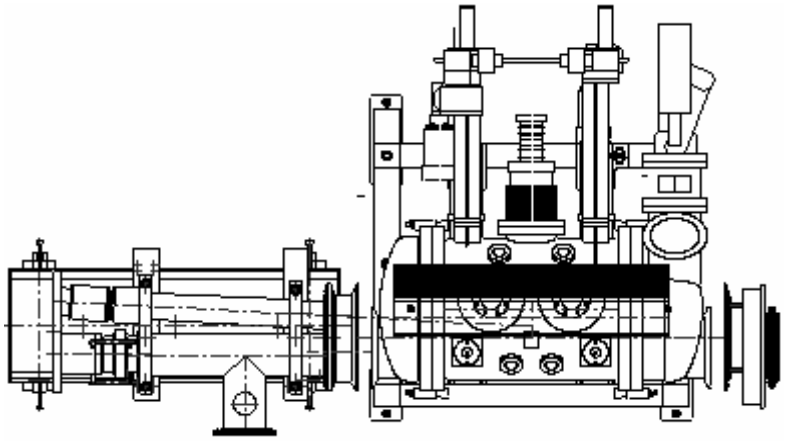

Figure 37.5: Layout of the PS straight-section 26 with the future ion injection septum

The connecting flange and flange aperture on the vacuum vessel will be increased, at least on the upstream side, to allow the injected beam to pass. In Fig. 37.5 the layout of the septum magnet and its vacuum vessel are illustrated. Experience with magnets of the same design has shown that the fringe field at the axis of the orbiting beam (approximately 50 mm from the septum) is below 0.15 % of the integrated gap field.

Table 37.5: Main parameters for PI.SMH26.

Deflection angle (maximum)	55 mrad
Integrated magnetic field (∫Bdl)	0.264 Tm
Gap field	0.336 T
Gap height	60 mm
Gap width between conductors	102 mm
Length (physical)	850 mm
Length (magnetic)	785 mm
Septum thickness	5 mm
Number of conductor turns	1
Peak current	16 kA
Half sine pulse base width	3 ms
Magnet inductance	1.8 μH
Magnet resistance	0.1 mΩ

The vacuum design relies on standard PS equipment, such as vacuum seals, vacuum pumps, and an under-vacuum bake out system. A vacuum in the low 10^{-9} mbar range is expected after a 5-day bake out period (of which 24 hours at 200 °C for the magnet core). The magnet is built as a modular plug-in unit, and can be exchanged for its spare within one day in the event of a failure. On the downstream side, space is available in the vacuum tank to insert a beam observation system (for example a scintillator screen). The mechanical displacement system will be recovered from the old "PE.SMH58" device. This system is of the same type as the standard systems used for septa in the PS Complex. This allows the magnet position to be adjusted with ±10 mm with respect to the nominal position of 53 mm from the circulating beam. Also the septum angle can be adjusted from the nominal zero to 10 mrad angle with respect to the circulating beam.

The power converter (including the step-up transformer in the tunnel) for the new pulsed injection septum magnet is discussed in Sec. 35.8.

37.3 UPGRADED INJECTION KICKER AND BUMPERS

Table 37.6: PS KFA28 System – Principal parameters after upgrading for ions

HV modulator:	Generator impedance:	12.5 Ω
	PFN:	4 RG220, 50 Ω, ~220m cables in parallel
	Transmission:	4 RG220, 50 Ω, ~150m cables in parallel
	Main Switch:	E2V CX1573
	Dump Switch:	E2V CX1573
	Max. PFN voltage:	35 kV (positive)
	Max. load current:	2800 A
Magnet:	Type:	lumped inductance
	Aperture w×h:	159 mm×70 mm
	Aperture centre shift:	25 mm outside from circulating beam centre line
	Effective length:	954 mm
	Useful field region	±0.5%: w=±62 mm, h=±27 mm from centre
	Inductance:	2.9 μH
Kick:	∫Bdl max:	46.5 mTm
	∫Bdl flat top uniformity:	± 0.5%
	∫Bdl post pulse ripple	±1%
	Deflection angle:	9.7 mrad
	Rise time (1-99 %):	1.1 μs
	Fall time (99-1 %):	1.15 μs
	Fall time (98-2 %):	940 ns
	Length (max):	~1 μs (variable)

The ion beam arriving from LEIR will be injected into the PS using the existing KFA28 kicker magnet. This is a lumped inductance single turn device using a window frame magnetic circuit, the bottom block of which is interrupted at the vertical median plane to reduce the inductive coupling between beams and magnet. The magnet is installed in the machine vacuum. It is connected to its high voltage generator via parallel strip lines within the vacuum tank and a coaxial vacuum feed-through at the tank wall. The magnet is short circuited at its other end inside the tank. This magnet was originally built for the antiproton beam extraction from PS to LEAR at $B\rho = 2.0$ Tm [5]. Injection at $B\rho = 4.8$ Tm requires an increase in the nominal integrated magnetic field to 330.4 Gm. This is possible as the ferrite magnetic circuit has sufficient cross section to avoid saturation, except in the magnet extremities where the effect is unimportant. The main data and performance of the PS ion injection kicker system are summarized in Tab. 37.6.

The increase in kick requires a new pulse generator. The proposed new system is shown in Fig. 37.6. The pulse-forming network (PFN) is charged to a maximum voltage of 35 kV and discharged by a thyratron switch into the magnet via a transmission line. A second thyratron switch is connected at the other end of the PFN to allow for pulse length adjustment.

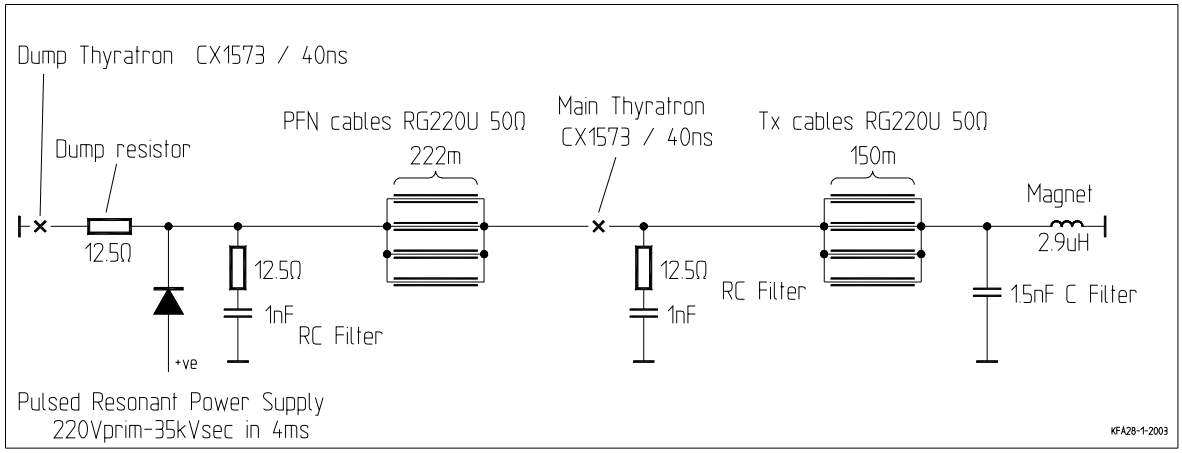

Figure 37.6: PS KFA28 system after upgrading for ions.

37.4 PS RF MANIPULATIONS FOR LEAD IONS

37.4.1 Overview

The role of the PS is to adapt the beam from LEIR according to a variety of constraints imposed by the downstream machines. Principally, the charge per bunch must be below the threshold for problems at injection in the SPS. But, in addition, it is the PS machine that imposes the bunch spacing required by LHC experiments, while the bunch length and repetition frequency at PS ejection must lie within the narrow ranges acceptable by the RF system of the SPS. The frequency window of the 200 MHz system of the SPS is shown in Fig. 37.7.

LHC experiments require that the bunch separation be some multiple of the 25 ns established for protons. If every m*th* SPS bucket is filled, then m must be a multiple of 5. Consequently, previously published scenarios concentrate on $m = 25$ with acceleration on PS harmonic $h = 17$ and extraction close to transition (γ_t=6.1) to obtain sufficiently short bunches. This is indicated by the point labeled "O" in Fig. 37.8. However, such schemes do not overcome the severe space charge problems at SPS injection so that a higher transfer energy and fewer charges per bunch are necessary. The point labeled "A" corresponds to the highest PS energy and also involves a factor of 5 in m. It may be reached by accelerating on $h = 21$, with $m = 20$ corresponding to a bunch spacing of 100 ns in the LHC. This spacing is preferable to 125 ns ($m = 25$) because the LHC bunch harmonic is then an integer, removing the need for turn-by-turn resynchronization by the experiments. Rebucketing from $h = 21$ to $h = 169$ using the PS 80 MHz cavities shifts the bunch repetition frequency within the scope of the SPS cavities (point "B"). Finally, bunch splitting from $h = 169$ to $h = 423$ using the PS 200 MHz cavities halves the number of charges per bunch and produces a beam ("C") that can be digested by the SPS. Of course, the resultant bunch pairs must be recombined at high energy in the SPS in order to re-establish both the 100 ns spacing and the intensity per bunch required for collisions in the LHC. In order to keep the total filling time reasonable, four bunch pairs are expected per PS cycle.

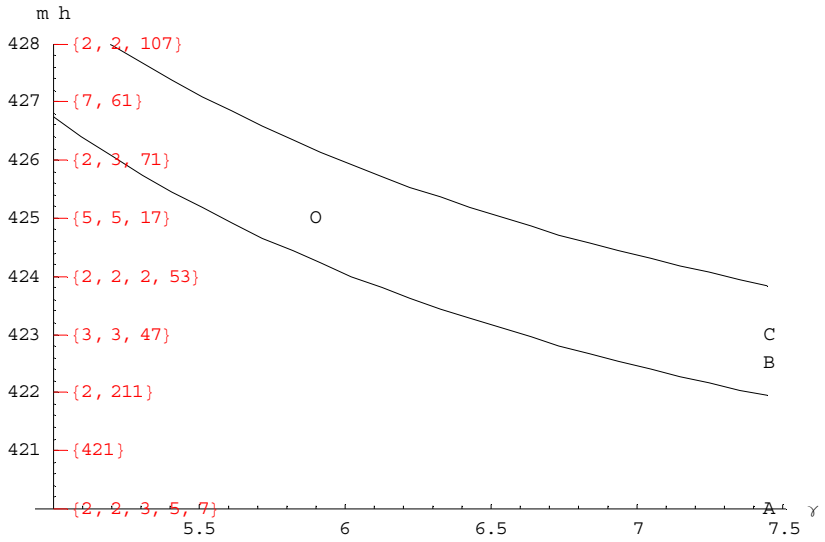

Figure 37.7: Upper and lower frequency limits of the SPS RF system as a function of relativistic factor γ for Pb^{54+} ions at PS extraction. The vertical scale gives the equivalent PS harmonic at 200 MHz and its prime factors.

37.4.2 Injection

The LEIR machine, operating on h = 2, delivers two bunches of lead ions to the PS at a magnetic rigidity of 4.8 Tm. This is just sufficient to allow the ferrite cavities of the PS to operate above their lower frequency limit (2.8 MHz) on h = 16 and hence for a bunch-to-bucket transfer between the two machines, whose size ratio is 8.

An injected bunch duration must not exceed 200 ns because a kicker gap of 150 ns between the two bunches at LEIR ejection is needed. A total (sum of all bunches) emittance of 0.1 eVs per nucleon allows a factor of 2 blow-up in the PS (Tab. 37.7). Under stationary transfer conditions, an RF voltage of 2.8 kV is then required in LEIR and is matched by 25 kV in the PS. Injecting into a moving bucket could also be considered in order to improve the energy reproducibility of the PS at transfer. Accelerating at a moderate 0.2 T/s, the bunches from LEIR could still be quite matched in the PS, but with insufficient longitudinal acceptance margin unless the LEIR RF voltage is raised to the 4 kV maximum available from one cavity. The shorter bunches imply 39 kV in the PS. At higher ramp rates, the spare LEIR cavity would have to be brought into operation.

37.4.3 Intermediate Energy Gymnastics

The beam is first accelerated on h = 16 to escape the space charge regime near injection ($\beta\gamma^2 = 0.43$). Then, on a magnetic plateau at around 22 Tm ($\beta\gamma^2 = 3.8$), the harmonic number is changed to 21 in a series of quasi-adiabatic steps while the number of bunches is doubled to four. The bunch spacing is initially increased during this “batch expansion” process, which is possible because the full circumference of the machine is not occupied.

The steps involved are harmonic number changes from h = 16 to h = 14 to h = 12 (each at 10 kV), then bunch splitting to h = 24 (at 15 kV) and, finally, to h = 21 (at 15 kV). All of this can be achieved in roughly 100 ms. The use of h = 24 means that the upper frequency limit (10.1 MHz) of the ferrite cavities precludes a higher intermediate energy.

37.4.4 Transition Crossing

A fast transition jump with a quasi-zero tune shift is a routine operation for proton beams in the PS to prevent particle loss and emittance growth triggered by instabilities. The elements in the ring comprise two “gamma jump cells”, each consisting of four quadrupole doublets separated into two families (the two central doublets of a cell together form a quadrupole triplet). Fig. 37.8 depicts the present layout [6].

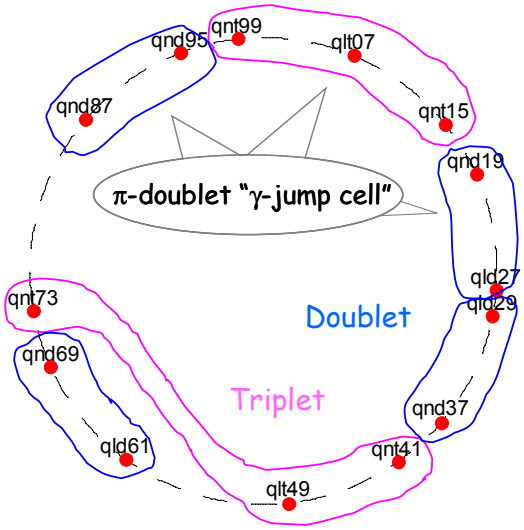

Figure 37.8: Quadrupole layout of the PS transition jump scheme.

At the ion intensities required for the LHC, neither longitudinal nor transverse microwave instabilities caused by the longitudinal broadband impedance are expected close to transition ($\gamma_t = 6.12$) [7]. Nevertheless, the transition jump system will still be used as a precautionary measure. Since the quadrupoles can only be powered with the currents used for protons, a gamma transition excursion of less than 0.1 is the maximum that can be achieved at the 72 Tm magnetic rigidity of lead ions at transition. A simulation of the transition jump process is shown in Fig. 37.9.

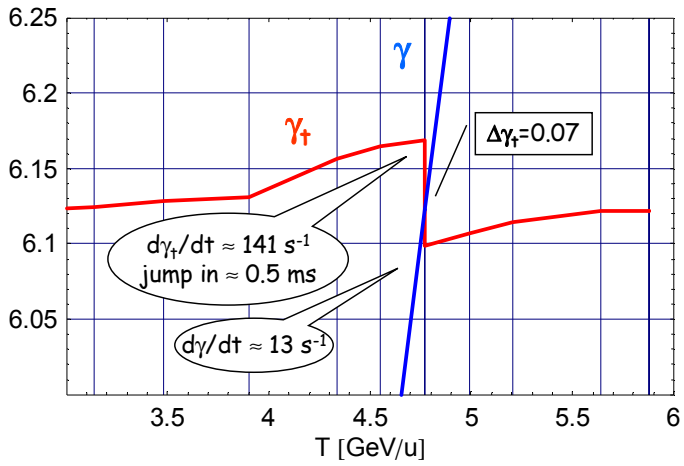

Figure 37.9: Relativistic γ versus kinetic energy for lead ions crossing transition in the PS (γ_t=6.12).

37.4.5 High-Energy Gymnastics

At top energy (86.7 Tm), the four bunches in consecutive h = 21 buckets are transferred from the ferrite cavity system (at 20 kV) to the fixed-frequency 80 MHz one (at 50 kV). In 80 MHz terms, there is a harmonic number change from h = 168 to h = 169 and the bunches are 8 buckets apart.

Optionally, if space charge proves problematic at injection in the SPS, the bunches could be split into pairs of consecutive buckets of the 200 MHz system (at 75 kV). In 200 MHz terms, there is a slight shift from h = 422.5 to h = 423, but this is insufficient to seriously bias the splitting equality. The final bunch pattern sees 5 ns between the "bunchlets" of each pair and 95 ns between the nearest neighbours of consecutive pairs. Note that h = 21 to 423 cannot be done in a single step because splitting requires that the ratio of harmonics be fairly close to 2.

The flat-top required for these manipulations is of the order of 125 ms, not including synchronisation with the SPS.

37.4.6 PS Longitudinal Parameters

Table 37.7: Summary of longitudinal beam characteristics at PS input and output.

Parameter at PS	Injection	Ejection 8 bunchlets	Ejection 4 bunches
Total number of ions	9×10^8	4.8×10^8	4.8×10^8
Number of bunches	2	4×2	4
Harmonic number	16	423	169
Total emittance [eVs per nucleon]	2×0.05	8×0.025	4×0.05
Bunch spacing [ns]	352	5+95	100
Bunch duration [ns]	202	3.9	3.9
RF voltage [kV]	25	75	75
RF frequency [MHz]	2.842	200	80
Dipole magnetic field [T]	0.0685	1.237	1.237
Equivalent proton momentum [GeV/c]	1.44	25.98	25.98

37.4.7 Early Lead Ion Operation Scheme

A simplified scheme has been proposed [8] for the first LHC ion run in which only one bunch of 2.25×10^8 ions in 0.025 eVs per nucleon is supplied to the PS by LEIR, which would operate on h=1 instead of h=2. The beam must be cooled to the same longitudinal density as before, but the lower intensity implies a shortening of the LEIR cycle from 3.6 to 2.4 s. The ramp rate at injection in the PS could be increased up to 0.6 Ts^{-1} without requiring the spare LEIR cavity. More significantly, no complicated RF gymnastics would have to be set up in the PS. Acceleration would take place uninterrupted on h = 16 and, after rebucketing at 80 MHz, a single bunch of 1.2×10^8 ions in 0.05 eVs per nucleon (again allowing a factor of 2 blow-up margin) would be extracted towards the SPS.

37.5 PS-SPS LINE STRIPPING WITH LOW-BETA INSERTION

The Pb^{54+} ion beams will be accelerated in the PS to 5.9 GeV/u (beam rigidity Bρ = 86.7 Tm) and then ejected and fully stripped to Pb^{82+} (Bρ = 57.1 Tm) in the TT2/TT10 transport channel between PS and SPS. This PS extraction energy, higher than the existing fixed target ion programme requires, has been chosen to avoid the limitations of space charge and of intra beam scattering at SPS injection. The implementation of a low-β insertion to minimise transverse emittance blow-up due to multiple Coulomb scattering in the stripping foil has been studied. In the presence of non-zero dispersion at the foil, the stripping process also leads to additional emittance increase due to energy straggling of the ions [9, 10]. The performance of the new low-β stripping insertion is compared to the current situation where the stripper is at a location with a relatively large betatron function and with the energy of 4.25 GeV/u instead of 5.9 GeV/u.

37.5.1 Emittance Budget of the LHC Lead Ion Beam

The transverse emittance budget of the ion beams to obtain the required luminosity for the lead experimental programme in the LHC is listed in Tab. 37.8.

Table 37.8: Normalized r.m.s emittance budget for the LHC ion and proton programmes and for the present operational beams.

MACHINE (at top energy)	Ions for LHC $\varepsilon^*_{h,v}$ [μm]	Protons for LHC $\varepsilon^*_{h,v}$ [μm]	Ions for SPS fixed target exp. $\varepsilon^*_{h,v}$ [μm]
LHC	1.5	3.75	-
SPS	1.2	3.5	4.0
PS	1.0	3.0	3.8
LEIR	0.7	-	-
BOOSTER	-	2.5	3.0

The PS emittance of $\varepsilon^*_{h,v} = 1.0$ µm (normalized r.m.s emittance $\varepsilon^*_{h,v} = \beta\gamma\sigma^2_{h,v}/\beta_{h,v}$, where $\sigma_{h,v}$ is the standard deviation of the projected distribution), or $\varepsilon_{h,v} = 0.18$ µm (physical r.m.s), refers to the value at the end of the TT2 transfer line after the stripping process. Small emittances (about 1/4 to 1/3 of the present lead ion beam emittances) are required. Thus emittance preservation is of great importance.

37.5.2 Present Situation in TT2

In the fixed-target lead ion runs performed up to now the charge state of the ions is changed from 53+ to 82+ in TT2 at 4.25 GeV/u ($B\rho = 66.7$ Tm for 53+) using a 0.8 mm thick aluminium stripping foil installed at about 302 m from the entrance of TT2. The betatron and dispersion functions of the entire TT2 transfer line for the present optics are shown in Fig. 37.10.

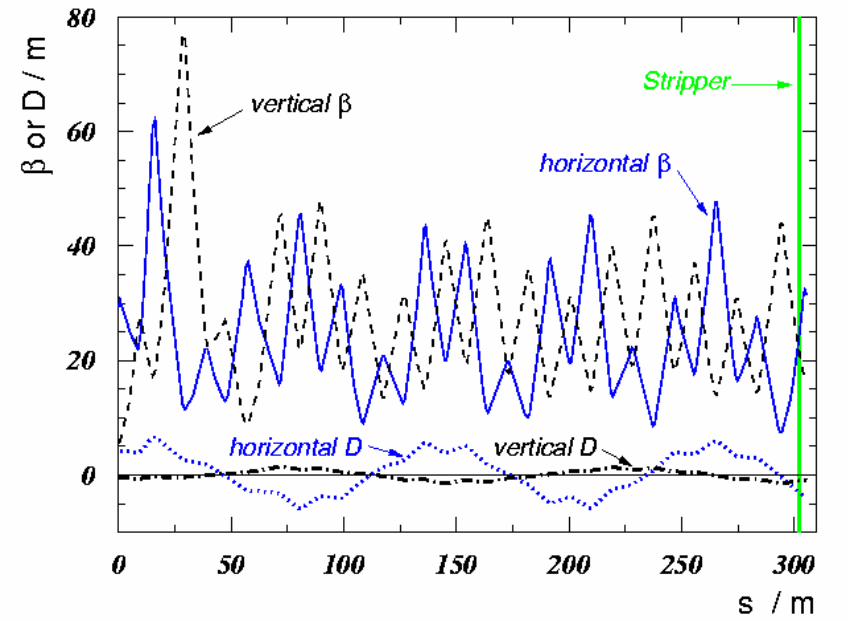

Figure 37.10: Horizontal and vertical betatron and dispersion functions of the present lead ion optics in TT2 transfer line (distance from entrance of TT2).

The quadrupole setting yielding the present optics has been kept in operation since the 1999 lead ion run following the 1998 matching campaign of the TT2/TT10 transfer line optics. A further re-matching was not retained because no conclusive result could be drawn from the measurements collected [11].

Measurements of the emittance growth due to stripping were performed in 1995 for a 0.8 mm thick aluminium foil. The measured transverse normalized r.m.s emittance increases at 4.25 GeV/u were about 0.59 to 0.77 µm [12] while calculations for this situation give about 0.42 to 0.45 µm (Tab. 37.11). While tolerable in the present fixed target runs ($\varepsilon^*_{h,v}$=4 µm as shown in Tab. 37.8), this blow-up is unacceptable compared to the $\varepsilon^*_{h,v}$=1.5 µm required at LHC collision energy.

37.5.3 The Proposed Low-β Insertion in TT2

A low-β insertion is proposed at about 70 m from the entrance of TT2, just before the beginning of the quadrupole string (families QDE210.S and QFO215.S). Detailed studies show that the existing quadrupoles are insufficient to match Twiss parameters and dispersion functions. To create the insertion, four quadrupoles are added and in addition the first two quadrupoles of the string have to be powered individually. Fig. 37.11 depicts betatron and dispersion functions of the proposed lead ion optics for the TT2 line. The optical functions at the new stripper (STRN) and at present stripper (STR373) are given in Tab. 37.9.

Since the optics parameters at TT2 entrance have been derived from measurements [11] they are subject to intrinsic uncertainties. However the proposed optics is flexible enough to guarantee stable conditions at the stripper for a reasonable range of initial parameters. Furthermore it has been shown that the emittance blow-up due to an imperfect re-matching of TT10 is small [10]. The betatron functions and therefore the emittance

blow-up due to multiple Coulomb scattering are reduced by about a factor five (Tab. 37.9) compared to the present optics.

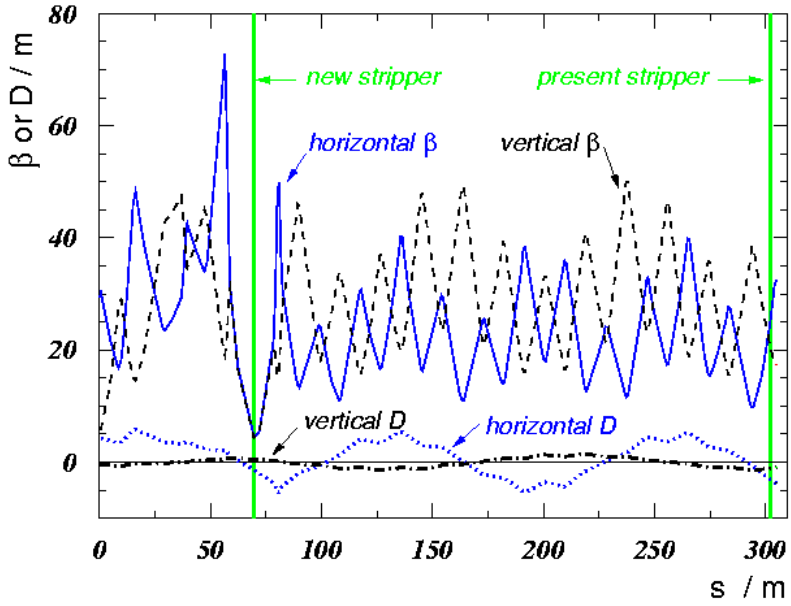

Figure 37.11: Betatron and dispersion functions of the new lead ion optics in the TT2 line with a low-β insertion (distance from entrance of TT2).

Table 37.9: Optical parameters at the present (STR273) and new stripper position (STRN)

Location	Horizontal				Vertical			
	β_h[m]	α_h	D_h[m]	D'_h	β_v[m]	α_v	D_v[m]	D'_v
Entry TT2	29.42	-2.51	4.13	0.41	5.71	0.29	-0.47	0.03
Present STR373	23.56	-1.70	-2.94	-0.34	22.05	1.12	-1.03	0.06
New STRN	4.92	-0.04	-1.33	-0.29	4.37	0.007	0.20	-0.08

Together with the increase of the PS extraction kinetic energy from 4.25 to 5.9 GeV/u the emittance growth due to the stripping process is reduced by roughly a factor six compared to the present optics. The impact of a thinner stripper foil (e.g. 0.5 instead of 0.8 mm) is shown in Tab. 37.10, the gain in emittance blow-up is about a factor two, at the expense of a drop in the stripping efficiency (96% to 83%) [12]. Thus, this is not an alternative to the low-β insertion.

Table 37.10: Scaling of normalized emittance blow up when stripping from Pb^{54+} to Pb^{82+}.

Kinetic energy	4.25 GeV/u	5.9 GeV/u	5.9 GeV/u
Stripper thickness d	0.8 mm	0.8 mm	0.5 mm
Emittance blow up ratio $\frac{d}{\beta^3\gamma} \Big/ \left(\frac{d}{\beta^3\gamma}\right)_{\text{at 4.25 GeV/u}}$	1	0.745	0.466

The influence of the non-zero dispersion at the stripper may lead to an additional emittance contribution after filamentation due to coherent energy loss of the ions crossing the stripper. This effect can be avoided by adjusting the optics downstream of the stripper for the lower reference momentum. Finally, the energy spread introduced by the straggling process for the thick aluminium foil (0.8 mm) yields a relative momentum spread of only $\sigma_p/p \approx 4\times10^{-5}$ at 5.9 GeV/u and is negligible.

Tab. 37.11 shows the calculated emittance growth for the present and the proposed low-β optics (assuming fully stripped lead ions) and for the measured [12] and "scaled" low-β optics.

Table 37.11: Increase in normalized r.m.s emittances in the stripper foil (0.8 mm Al) for the present optics of lead ions (4.25 GeV/u) and new low-β optics (5.9 GeV/u).

Optics	$\Delta \varepsilon^*_h$ [mm]		$\Delta \varepsilon^*_v$ [mm]	
	Scattering	Straggling	Scattering	Straggling
Calculated present	0.447	0.003	0.418	0.0002
Calculated low-β	0.069	0.004	0.062	0.0003
	Scattering + straggling		Scattering + straggling	
Measured present	0.766		0.584	
"Scaled" low-β	0.119		0.086	

37.6 STRIPPING IN THE PS-SPS LINE: HARDWARE ASPECTS

37.6.1 Quadrupole Layout for the Present Situation

The quadrupoles used for the present optics with their characteristics are listed in Tab. 37.12. QDE210.S and QFO215.S denote a string made of two families of quadrupoles arranged as a FODO lattice, each family being powered by a single power supply. Families QDE210.S and QFO215.S comprise 14 and 13 quadrupoles, respectively. The first seven quadrupoles in TT2 are used for matching purpose.

Table 37.12: TT2 quadrupole characteristics for the present optics and low-β optics, (1) indicates new quadrupoles, (2) new power supplies.

Quadrupole	Type	Present optics		Low-β optics		Comments
		Strength	Current	Strength	Current	
QF0105	-	7.26 T	345.7 A	10.72 T	510.4 A	
QDE120	QFL	-8.23 T	-160.4 A	-10.81 T	-208.1 A	
QFO135	QFL	7.91 T	154.2 A	7.46 T	145.0 A	
QDE150	QFL	-6.32 T	-123.1 A	-5.56 T	-108.2 A	
QNO01 (1) (2)	QFS			-3.18 T	-91.2 A	In stock
QFO165	QFL	5.85 T	114.1 A	9.32 T	181.0 A	
QDE180	QFL	-5.30 T	-103.3 A	-7.38 T	-143.5 A	
QFO205	QFL	5.80 T	113.1 A	20.81 T	422.9 A	
QNO02 (1) (2)	QFL			-19.48 T	389.7 A	In stock
New stripper						
QDE210 (2)	QD	-6.02 T	-169.1 A	-0.40 T	-11.3 A	
QNO03 (1) (2)	QFS			-11.95 T	-347.5 A	In stock
QFO215	*QFS*	6.56 T	188.6 A	*20.36 T*	*Overflow*	*To be moved*
QFO215 (2)	QFL			20.36 T	411.3 A	New: in stock
QNO04 (1) (2)	QFS			-7.82 T	-223.4 A	Old QFO215
QDE210.S	QD	-6.02 T	-169.1 A	-4.80 T	-134.7 A	
QFO215.S	QFS	6.56 T	188.6 A	5.37 T	153.5 A	
Present stripper						
QFO375	QFS	3.70 T	106.2A	4.40 T	125.9 A	

37.6.2 Quadrupole Characteristics for the Low-β Insertion

The proposed layout for the low-β insertion with its characteristics is given in Tab. 37.12. The maximum strengths for the three types of quadrupoles proposed QFS (L = 0.8 m), QD (L = 0.82 m) and QFL (L = 1.2 m) are 15.64, 16.66 and 23.20 T, respectively. QFO215 (to be disconnected from family QFO215.S) will be

transferred to the QNO04 location where a lower gradient is required and replaced by a longer quadrupole. The characteristics of the six new power converters needed for TT2 are described in Sec. 36.4. The location of the new quadrupoles in TT2 is given in Tab. 37.13.

Table 37.13: TT2 new quadrupole positions (values refer to the quadrupole entry). The new stripper foil (STRN) will be located at 69.59 m from the entry of QF0105.

New quadrupole	QNO01	QNO02	QNO03	QNO04
Position from entry QF0105	37.00 m	58.52 m	78.29 m	81.75 m

The new magnetic structure and optics are shown in Fig. 37.12 which is a zoom into the first 90 m of TT2. The shaded elements represent the additional four quadrupoles required.

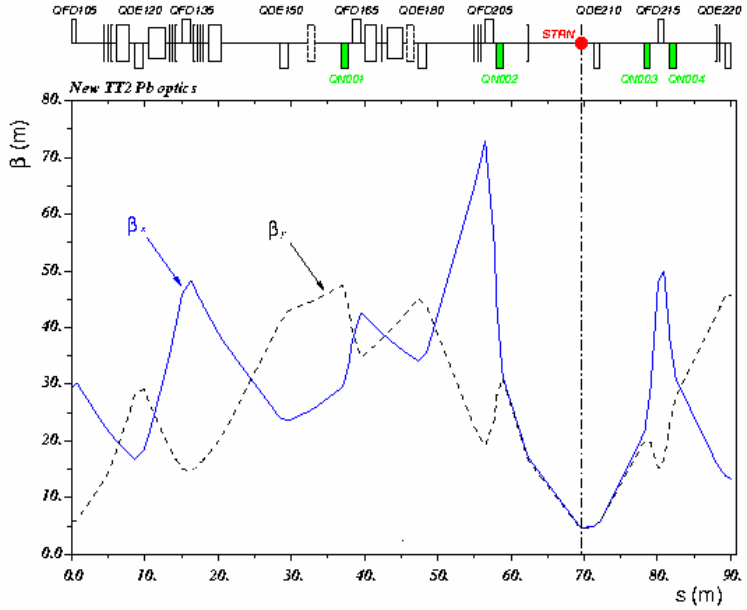

Figure 37.12: A zoom on the first 90 m of the TT2 line with the low-β insertion optics.

REFERENCES

[1] M. Martini, *Injection of the lead ion beam for LHC into the PS,* PS/AE Note 2001-012, 2001.

[2] R. Garoby, S. Hancock, *LHC Ion Bunch Generation in the PS,* Proc. CERN/PS/RF/Note 2002-10.

[3] D. Cornuet, Z. Sharifullin, *Magnetic Measurements on the PS Magnet Unit U17 with Hall Probes,* AT/MA Note 92-23, 1992.

[4] H.H. Umstätter, *Simple Formulas for Fringe Field of PS-Magnet,* PS/SM/Note 77-12, 1977.

[5] D.C. Fiander, K.D. Metzmacher, D. Grier, *Simple proposal for a kicker for the fast extraction of antiprotons from SS 26,* PS/EI/Note 80-9.

[6] T. Risselada, "Gamma transition jump schemes", CERN 94-01, pp313–327 (1994).

[7] A.W. Chao and M. Tigner (Editors), "Handbook for Accelerator Physics and Engineering", pp281–283 (1999).

[8] J. Poole (Editor), "Proceedings of the workshop on LHC performance – Chamonix XII", pp11–12, CERN-AB-2003-008 ADM (2003).

[9] L. Durieu, M. Martini, S. Maury, D. Möhl, A-S Müller, *A Low-β stripping insertion in the PS-SPS transfer line to limit emittance blow-up due to stripping of lead ions for LHC*, CERN-PS-2001-006 (AE).

[10] M. Giovannozzi, M. Martini, A-S Müller, *A Low-β stripping insertion in the CERN PS to SPS transfer line for the LHC ion programme*, Proc. PAC'01, Chicago, June 2001, CERN-PS-2001-036 (AE).

[11] G. Arduini et al., *Betatron and dispersion matching of the TT2/TT10 transfer line for the fixed target lead ion beam*, CERN PS/CA Note 99-009.

[12] G. Arduini et al., *Lead ion beam emittance and transmission studies in the PS-SPS complex at CERN,* Proc. EPAC'96 Sitges, Spain, 1996.